IEEE Access
Multidisciplinary | Rapid Review | Open Access Journal

Received 24 February 2023, accepted 11 March 2023, date of publication 17 March 2023, date of current version 22 March 2023.

Digital Object Identifier 10.1109/ACCESS.2023.3258545

RESEARCH ARTICLE

Multifunctional Bandpass Filter/Displacement Sensor Component

ZAHRA SHATERIAN[1,2], (Member, IEEE), AND MICHAL MROZOWSKI[2], (Fellow, IEEE)

[1]Department of Electrical Engineering, Technical and Vocational University (TVU), Tehran 14357-61137, Iran
[2]Department of Microwave and Antenna Engineering, Faculty of Electronics, Telecommunications, and Informatics, Gdańsk University of Technology, 80-233 Gdańsk, Poland

Corresponding author: Zahra Shaterian (z.shaterian@gmail.com)

This work was supported by the Polish National Science Center under Grant UMO-2019/33/B/ST7/00889.

ABSTRACT This paper presents the design and realization of a multifunctional bandpass-filter/displacement-sensor using an edge-coupled microstrip bandpass filter loaded by a pair of split ring resonators (SRRs). It is shown that while the structure acts as a bandpass filter at its operating frequency, the phase of the reflection coefficient from a movable loading resonator at the resonance frequency of the resonator can be used for displacement sensing. With this aim, and to avoid any interference with the filter functionality, the resonance frequency of the SRRs is chosen within the stopband of the bandpass filter, where all the input signal is reflected back to the input port. Therefore, moving the loading resonators does not have any adverse effect on the filtering performance. To validate the concept, a fifth-order Chebyshev bandpass filter with a feed line loaded with a pair of SRRs is designed and the numerical evaluation of the proposed multifunctional bandpass-filter/displacement-sensor is provided. The proposed multifunctional component is also validated through fabrication and measurement. It is shown that the proposed component has a sensitivity of 8°/mm at the designed frequency of SRRs. However, the sensitivity can be increased by scaling the SRRs to resonate at a higher frequency within the upper stopband of the filter.

INDEX TERMS Bandpass filter, displacement sensor, multifunctional microwave component, phase, split ring resonator (SRR).

I. INTRODUCTION

New wireless systems intended for the mass market need a large number of compact, lightweight, and low-cost microwave components. In response to this demand, multifunctional microwave components that combine several components with different functionalities into a single device have been developed in many studies. Some examples of multifunctional microwave components are filtering antennas [1], [2], [3], filtering power amplifiers [4], [5], [6], filtering power dividers [7], [8], [9], [10], [11], and filtering switches [12]. As seen in the above-cited studies, the development of multifunctional components composed of a filter and another passive component has been a hot research topic in recent years. This is because filters are important passive components in the radio-frequency (RF) front-end of almost all wireless communication systems.

On the other hand, microwave sensors have several advantages including low-profile, high sensitivity, and robustness to harsh environmental conditions, which make this type of sensors attractive for various applications such as material characterization [13], [14], defect detection [15], [16], [17], [18], bio-sensing [19], microfluidics [20], ambient monitoring [21], rotation sensing [22], [23], [24], [25], [26], [27], [28], displacement sensing [29], [30], [31], [32], [33], [34], [35], [36], [37], [38], [39], etc. Moreover, microwave sensors have intrinsic potential for application in wireless systems, which use electromagnetic (EM) waves for data transmission. Thus, with the advent of the internet of things (IoT) technology, which is expected to satisfy a large number of wireless connectivity requirements for today's applications, the use of microwave sensors has experienced exponential growth.

The associate editor coordinating the review of this manuscript and approving it for publication was Derek Abbott.

Although filters and sensors are two indispensable microwave components, surprisingly few studies on the integration of filter and sensor components have been conducted. However, new multifunctional RF circuits with filtering/sensing capabilities are required, especially in IoT networks, where the collected data from various sensors need to be processed and sent through a wireless communication system. The first attempt to address the demand for multifunctional filter/sensor components has been presented in [40]. The filter/sensor proposed in [40] is an ultra-wideband (UWB) filter that features a controllable transmission zero within the passband region. The position of this transmission zero is changed by adjusting the angular displacement of a rotatable section. Therefore, the angular displacement can be determined by measuring the frequency of the transmission zero. Despite its acceptable performance in UWB systems, the method cannot be used for combining sensors and narrowband filters. To extend the design of multifunctional filter/sensor components for narrowband applications, authors very recently proposed a method for the design of multifunctional bandstop-filter/sensor components in [41]. In the method proposed in [41], resonators which are the main building blocks of the filter are also used for sensing. Therefore, the operating frequency of the sensor is identical to the center frequency of the filter. However, to avoid adverse mutual effects between the filtering and sensing functionalities, sensing is conducted based on the phase of a reflected signal, while the amplitude-frequency response, which is important for filtering, is untouched.

The main limitation of the method proposed in [41] is that it is only applicable for the integration of microwave sensors and bandstop filters. This is because the structure of the bandstop filter is composed of a through transmission line loaded with resonators. Hence, as long as the spacing between the resonators is fixed, their displacement as a group does not affect the bandreject behavior. In contrast, a bandpass filter is composed of several coupled resonators that are also coupled to the source and load terminations. Therefore, while displacing the coupled resonators (as a whole) does not change the inter-resonator couplings, it alters the couplings of the first and last resonators to the source and load. Moreover, note that in contrast to the bandstop filter, the reflection coefficient of a bandpass filter in its passband region is too low and the phase of the reflection coefficient within the passband cannot be precisely measured. Therefore, the main objective of this paper is to further extend the method for integrating bandpass filters and sensors. With this aim, a novel method for the design of multifunctional bandpass-filter/displacement-sensor components is proposed. To perform simultaneous sensing and bandpass filtering the sensing is conducted based on the variations of the phase of the reflection coefficient at the resonance frequency of a resonator, which is adjusted to occur at a frequency in the stopband of the filter. Therefore, the passband response of the filter remains intact. For demonstration, a fifth-order edge-coupled bandpass filter integrated with a displacement sensor based on a pair of split ring resonators (SRRs) is presented. Note that the size of the filter/sensor component can be drastically reduced if compact filters such as those based on split ring resonators are utilized. However, as the objective of this research does not prioritize size reduction, a conventional coupled line bandpass filter has been employed.

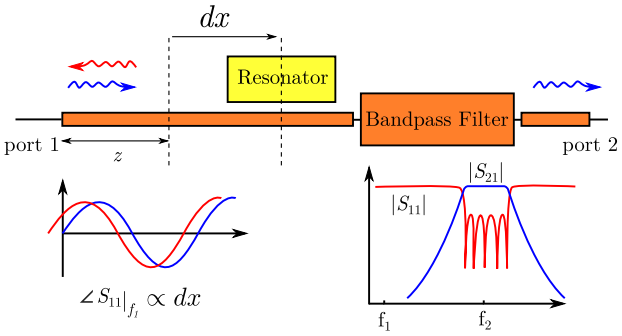

FIGURE 1. The block diagram of the proposed method for designing multifunctional bandpass-filter/displacement-sensor component.

II. PRINCIPLE OF OPERATION AND NUMERICAL VALIDATION

In this section, the principle idea, design, and numerical validation of the proposed multifunctional bandpass-filter/displacement-sensor component are presented.

A. PRINCIPLE IDEA OF BANDPASS-FILTER/DISPLACEMENT-SENSOR

Fig. 1 shows the block diagram of the proposed method. As shown in the figure, the proposed structure is composed of a bandpass filter with a feed line loaded with a resonator. The filter is realized on one substrate, whereas the resonator is realized on a second substrate, and thus can be displaced along the feed line. Assuming that the resonance frequency of the resonator is outside the passband of the filter, any signal within the frequency band of the bandpass filter ideally reaches the second port with no attenuation. In contrast, if a signal within the stopband spectrum of the filter (excluding signals at the resonance frequency of the resonator) is fed to port 1, it will be reflected back by the filter. However, it is important to note that a signal at the resonance frequency of the resonator f_r is reflected back by the resonator before reaching the filter. Therefore, provided the line is matched to the port, when the resonator is located at its initial position (as indicated by $dx = 0$ in Fig. 1), the phase of the reflected signal at the resonance frequency f_r of the resonator is $\angle S_{11} = -2\beta_{f_r} z$, where z is the length of the microstrip line from the initial position to port 1, $\beta_{f_r} = \beta_0\sqrt{\epsilon_{eff}}$ is the phase constant of the microstrip transmission line at f_r, and ϵ_{eff} is the effective permittivity for the microstrip line which is obtained by [42]:

$$\epsilon_{eff} = \frac{\epsilon_r + 1}{2} + \frac{\epsilon_r - 1}{2}\frac{1}{\sqrt{1 + 12h/w}}. \quad (1)$$

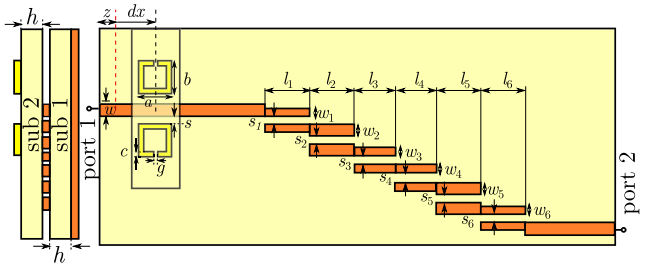

FIGURE 2. Side and top views of the proposed multifunctional bandpass-filter /displacement-sensor. The width of the microstrip line is $w = 0.52$ mm, which corresponds to a characteristic impedance of 50 Ω. The resonators have dimensions of $a = 14$ mm, $b = 10$ mm, $g = 0.3$ mm, $c = 0.3$ mm, and are spaced $s = 0.4$ mm apart from the microstrip.

In this equation, w and h are the width of the microstrip line and the thickness of the substrate with a relative permittivity of ϵ_r, respectively. As the resonator moves longitudinally by dx, the distance between port 1 and the resonator changes to $z + dx$, resulting in a change in the phase of the reflected signal to $-2\beta_{f_r}(z+dx)$. Thus, the amount of displacement is determined by measuring the phase of the reflection coefficient at the resonance frequency of the resonator. It is clear that the filtering behavior of the component at the operating frequency of the filter is untouched since the sensing is performed based on the variation of phase (rather than amplitude or frequency) at an arbitrarily selected frequency within the stopband of the filter.

B. FILTER/SENSOR DESIGN

To validate the concept, a fifth-order Chebyshev bandpass filter with the center frequency $f_0 = 2$ GHz, 10% fractional bandwidth (FBW), and 16.4 dB return loss in the passband is designed and simulated as the filter part, while a pair of SRRs on a different layer is used as the sensor part. In this design, the bandpass filter is realized using edge-coupled half-wavelength resonators. However, generally, any type of bandpass filter can be used for this purpose. Also, the pair of SRRs can be replaced with other types of resonators.

Fig. 2 illustrates cross-sectional and top views of the multifunctional bandpass-filter/displacement-sensor component. The structure is made up of two substrates stacked on top of each other, with a microstrip line and its ground plane on the top and bottom layers of the first substrate and a pair of SRRs on the top layer of the second substrate, as depicted in the figure. The second substrate is ungrounded.

The bandpass filter is designed based on a conventional procedure [43]. We assume that the filter is to be implemented as a simple coupled line structure. The designed parameters calculated based on the filter specifications are listed in Table 1. Note that due to the symmetry of the filter, only half of the parameters are shown in this table. For both substrates, the material utilized is Rogers *RO6010*, which has a relative permittivity of $\epsilon_r = 10.2$, a dielectric loss tangent of $\tan(\delta) = 0.0023$, and a thickness of $h = 0.508$ mm with 18 μm thick copper metallizations. Using the design

TABLE 1. Design Parameters of the Fifth-Order Coupled Line.

j	$J_{j,j+1}/Y_0$	$(Z_{0e})_{j,j+1}$ (ohms)	$(Z_{0o})_{j,j+1}$ (ohms)
0	0.370	75.353	38.343
1	0.125	57.047	44.521
2	0.095	55.228	45.682

TABLE 2. Microstrip Design Parameters of the Fifth-Order Coupled Line.

j	w_j (mm)	s_j (mm)	$(\epsilon_{re})_j$	$(\epsilon_{ro})_j$	l_j (mm)
1 and 6	0.29	0.2	7.087	5.735	14.85
2 and 5	0.41	0.53	7.311	5.976	14.585
3 and 4	0.42	0.68	7.297	6.052	14.546

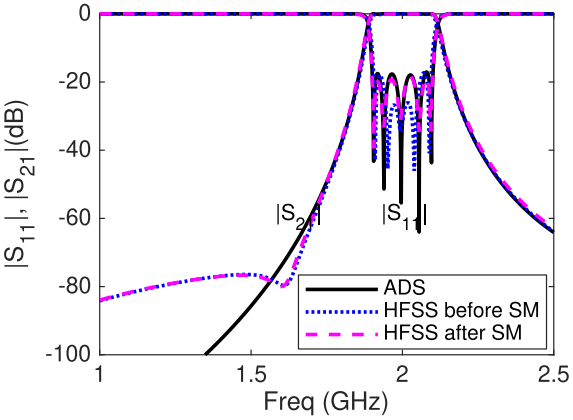

FIGURE 3. Circuit and EM simulated magnitude of the transmission and reflection coefficients of the designed filter with and without space mapping technique.

equations in [43], the width w_j, spacing s_j and the initial length l_j for each pair of quarter-wavelength coupled resonators are calculated as listed in Table 2. Other dimensions of the structure are as denoted in the caption of Fig. 2. Note that to obtain the actual length of each coupled line section the capacitive effect of the open ends of the resonators has to be considered. With this aim, and also to take other parasitic effects into account, all the calculated dimensions of the filter are optimized using the space mapping (SM) technique based on the co-simulation between the Advanced Design System (ADS) circuit simulation software and the full-wave High Frequency Simulation Software (HFSS). Fig. 3 depicts the circuit and the full-wave EM simulated magnitude of the transmission and reflection coefficients of the designed filter. As shown in this figure, an almost perfect agreement between the EM-simulated and circuit-simulated results is achieved by optimizing the dimensions of the filter using the space mapping technique.

As mentioned earlier, a pair of SRRs is used for displacement sensing. If the dimensions of the pair of SRRs are

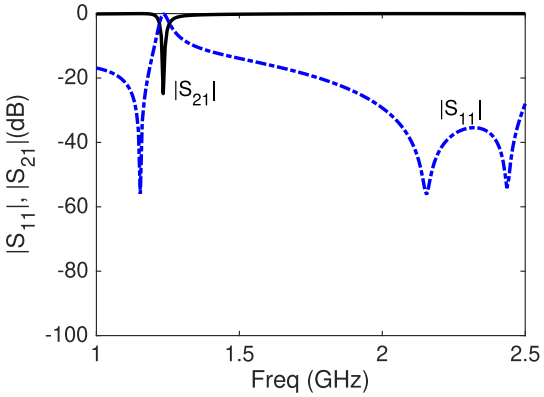

FIGURE 4. Magnitude of the transmission (solid line) and reflection (dashed line) coefficients for a pair of SRRs with dimensions as denoted in the caption of Fig. 2.

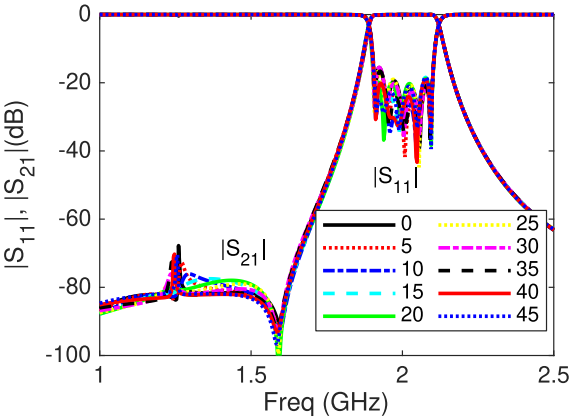

FIGURE 5. Simulated amplitude of the transmission and reflection coefficients for different values of displacement *dx* from 0 mm to 45 mm in steps of 5 mm.

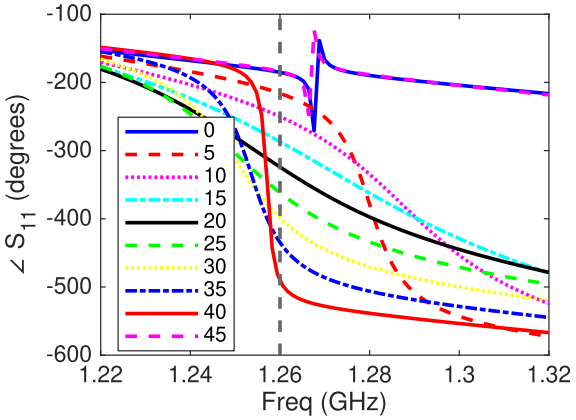

FIGURE 6. Simulated phase of the reflection coefficient for different displacement *dx* from 0 mm to 45 mm in steps of 5 mm.

adjusted such that they resonate at a frequency outside and relatively far from the passband region of the filter, their effect on the frequency response of the filter is negligible. At their resonance frequency, however, all the incident power is reflected back to port 1 by the resonators. Since the phase of the reflected signal depends on the location of the pair of SRRs, their displacement in the longitudinal direction changes the phase of the reflection coefficient at port 1. With these considerations in mind, the SRRs are designed to resonate roughly at $f_r = 1.26$ GHz. Fig. 4 shows the EM simulated transmission and reflection coefficients for the designed pair of SRRs with dimensions as denoted in the caption of Fig. 2. Note that caution must be exercised to design SRRs such that their second resonance frequency does not occur within or close to the passband of the filter. Satisfying this condition guarantees that the sensor has a minimum effect on the amplitude and the phase response of the bandpass filter.

C. NUMERICAL VALIDATION

Now using the designed pair of resonators and bandpass filter, the proposed multifunctional filter/sensor component as shown in Fig. 2 is numerically simulated in HFSS. The EM simulation results of the proposed device for different displacements dx ranging from 0 mm to 45 mm in 5 mm increments are illustrated in Figs. 5 and 6. Fig. 5 shows the amplitude of the transmission and reflection coefficients, while Fig. 6 depicts the phase of the reflection coefficient at port 1 (i.e., $\angle S_{11}$). It is evident from Fig. 5 that displacing the top layer has a negligible effect on the frequency response of the filter. The figure also shows that the signal entering port 1 reaches port 2 at the bandpass frequencies of the filter (centered at $f = 2$ GHz), while it is reflected back to port 1 at other frequencies. However, the incident signal at the SRRs' resonance frequency (which is within the stopband of the filter) is reflected back by the SRRs before reaching the filter. Therefore, its phase depends on the location of the SRRs, and hence it varies with their displacement dx (see Fig. 6). To sum up, the simulation results demonstrate that a displacement can be sensed by analyzing the phase of the reflected wave, while maintaining the amplitude response of the integrated filter unaffected. Note that due to the finite quality factor of the resonators, the phase of the reflection coefficient around the resonance frequency is a function of the displacement, and this effect disappears as moving away from the resonance frequency. It is also inferred from Fig. 6 that the sensing span of the designed sensor is about 45 mm since larger displacements result in phase ambiguity.

III. EXPERIMENTAL RESULTS

A prototype of the bandpass-filter/displacement-sensor is fabricated and measured to validate the simulation results. Fig. 7 illustrates the photograph of the fabricated prototype, which matches the dimensions of the simulated structure in Section II. The photograph in Fig. 8 depicts the measurement setup, which involves a linear translation stage for accurate adjustment of the top substrate in the x direction. A low-permittivity foam piece connects the top substrate,

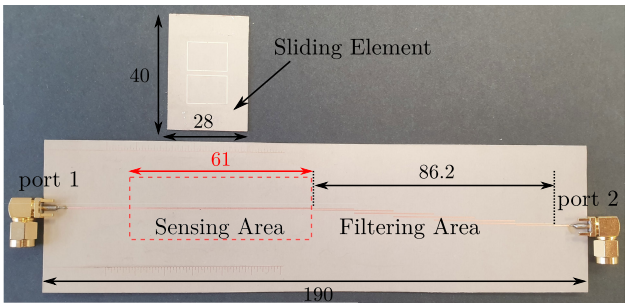

FIGURE 7. A photograph of the fabricated prototype. All dimensions are in mm.

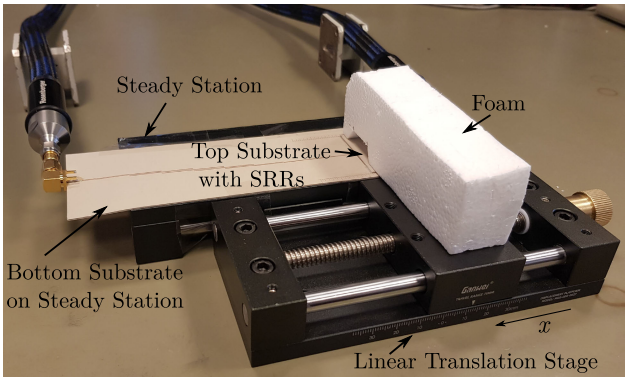

FIGURE 8. A photograph of the measurement setup. A piece of foam connects the top substrate, where the resonators are positioned, to the linear translation stage.

where the resonators are positioned, to the linear translation stage.

Fig. 9 shows the measured amplitude of the transmission and reflection coefficients for different values of displacement dx from 0 mm to 40 mm in steps of 5 mm. It also indicates the measured amplitude of the transmission and reflection coefficients of the proposed component without SRRs. As shown in this figure, the return loss is better than 10 dB, the center frequency is 1.9 GHz, and the FBW is 11.6%. The measured insertion loss at the center frequency of the filter for different values of displacement is between 2.5 dB to 2.8 dB, which is acceptable for a fifth-order microstrip filter with the mentioned FBW. The discrepancy between the simulated and measured results is mainly because the simulations were conducted using ideal dielectric and conductor materials. It is also attributed to a slightly different relative permittivity of the substrate material used in the fabricated prototype, which is around $\epsilon_r = 10.8$ rather than 10.2, the conductor loss, losses of the SubMiniature version A (SMA) connectors, and fabrication tolerances. Note that the notches in the reflection coefficient around the resonance frequency of the SRRs are due to the resonance-induced losses in the fabricated prototype. These notches are not present in the simulation results, as simulations were carried out using lossless materials (as seen in Fig. 5). Furthermore, as shown in Fig. 9, the notch

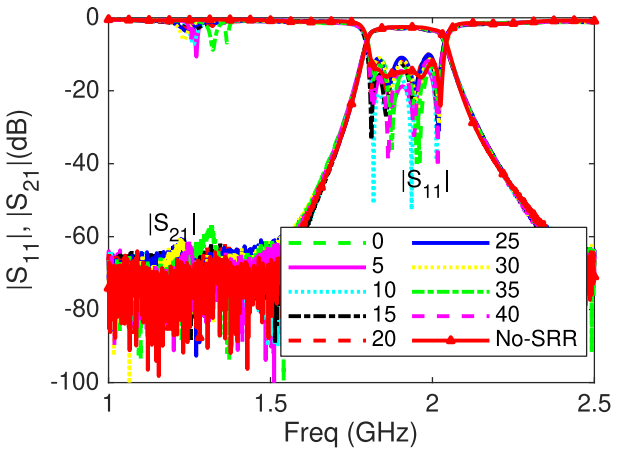

FIGURE 9. Measured amplitude of the transmission and reflection coefficients for different values of displacement *dx* from 0 mm to 40 mm by steps of 5 mm.

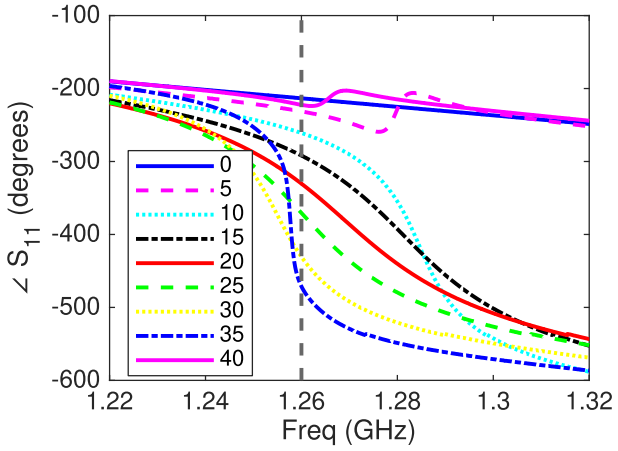

FIGURE 10. Measured phase of the reflection coefficient for different displacement *dx* from 0 mm to 40 mm by steps of 5 mm.

is not observed in the measured results without the SRRs. The measured phase of the reflection coefficient at port 1 for different values of displacement dx from 0 mm to 40 mm in steps of 5 mm is depicted in Fig. 10. This figure illustrates that as dx increases, the phase of S_{11} at 1.26 GHz decreases. Meanwhile, the magnitudes of the reflection and transmission coefficients (as shown in Fig. 9) remain mostly unchanged. According to Fig. 10, the sensor's measurement range is approximately 40 mm, which is slightly less than half of the guided wavelength.

Fig. 11 compares both the simulated and measured phase of the reflection coefficients versus displacement at the resonance frequency of the SRRs. This figure shows a good agreement between simulated and measured results. Since the experimental measurement span of the sensor is slightly less than the simulated one, this figure is shown for a range of 35 mm displacement. This figure also shows that the proposed sensor exhibits a linear response and has a sensitivity

TABLE 3. A Comparison Between the Proposed Bandpass Filter/Sensor and State-of-the-Art Sensors.

Reference	Sensor Type	Sensing Mechanism	Dynamic Range (° or mm)	Ave. Sensitivity	Frequency (GHz)	λ_g (mm)	Size (mm × mm)	Area (λ_g^2)	Type of Co-integrated Filter	FBW (%)
[35] Sensor A	Displacement	Phase variation	≈ 5 mm	35.14°/mm	2	90	70 × 20	0.15	-	-
Sensor B	Displacement	Phase variation	≈ 5 mm	95.24°/mm	2	90	70 × 20	0.15	-	-
Sensor C	Displacement	Phase variation	≈ 2 mm	312.97°/mm	2	90	92.5 × 20	0.23	-	-
[36]	Displacement	Frequency shift	7 mm	86 MHz/mm	1.98	121	≈ 22 × 10	0.015	-	-
[37]	Displacement	Phase variation	26.5 mm	13.5°/mm	15	26.5	41 × 23.2	1.35	-	-
[40]	Rotation	Frequency shift	90°	2.27 MHz/°	2.17	84.7	50 × 46	0.32	UWB	110
[41]	Displacement	Phase variation	18 mm	20°/mm	4.9	37	40 × 13	0.38	Bandstop	5.3
This work	Displacement	Phase variation	45 mm	8°/mm	1.26	92	147 × 22	0.37	Bandpass	10

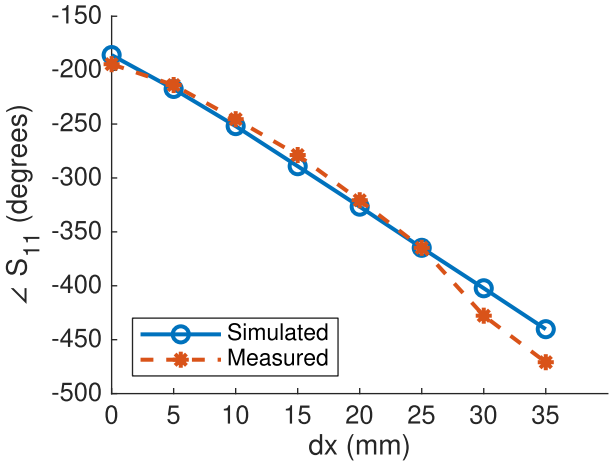

FIGURE 11. Simulated and measured phase of the reflection coefficients versus displacement *dx* at resonance frequency *f* = 1.26 GHz.

of approximately 8°/mm. Note that as long as the operating frequency of the sensor is outside the passband region of the filter, a compromise between the measurement span and the sensitivity of the sensor can be made by adjusting the operating frequency depending on the application. If high sensitivity (of course at the cost of a lower measurement span) is needed the SRRs can be designed to resonate in the upper stopband of the filter.

The proposed bandpass filter/sensor and the state-of-art filter/sensors in the literature are compared in Table 3. Since the multifunctional filter/sensors in the literature are limited to [40] and [41], additional displacement sensors based on phase variation in [35] and [37], and a displacement sensor based on frequency shift [36] are also included in the table. Note that while the first half of the table is dedicated to sensors that can only sense displacement, the second half showcases multifunctional filter/sensor components that are larger in size due to their added functionality. In short, the table shows that sensors in the [35] and [36] have smaller sizes, but they have a limited dynamic range. The sensor proposed in [37], which is based on gap waveguide technology, has a higher dynamic range and moderate sensitivity, but it operates at a higher frequency and is larger in size. The filter/sensor presented in [40], which is an angular sensor co-integrated with a UWB filter with 110% FBW, is based on the variations of the frequency (rather than phase) and has a sensitivity of 2.27 MHz/°. The table also shows the sensitivity and dynamic range of the multifunctional filter/sensor presented in [41] and the one presented in this study. The absolute values presented in the table show that the multifunctional filter/sensor presented in this study benefits from a higher dynamic range but lower sensitivity compared to [41]. However, normalized values of the dynamic range and sensitivity of both filter/sensors relative to the wavelength are identical. As mentioned earlier, by changing the operating frequency a higher absolute sensitivity can be achieved at the cost of a lower absolute dynamic range, and vice versa. It should be also noted that the normalized sensitivity of the filter/sensor presented in this work is double that of the sensor presented in [37] while its normalized dynamic range is half. This is because the sensor in [37] operates based on the phase of the transmission rather than the reflection coefficient.

IV. CONCLUSION

A new microwave multifunction device has been proposed that integrates two functionalities: that of a bandpass filter and that of a displacement sensor. The displacement is measured from the phase of the signal reflected by a pair of sliding SRR resonators placed at the input of the bandpass filter and tuned so that its first and second resonances are outside the passband of the filter. In this way, the resonance of the displacement-sensing SRRs do not interfere with the operation of the filter. To demonstrate the effectiveness of this approach, a 5th-order Chebyshev bandpass filter/displacement sensor was designed, fabricated, and measured. It is shown that there is good agreement between the simulation and the experimental results.

REFERENCES

[1] W.-J. Wu, Y.-Z. Yin, S.-L. Zuo, Z.-Y. Zhang, and J.-J. Xie, "A new compact filter-antenna for modern wireless communication systems," *IEEE Antennas Wireless Propag. Lett.*, vol. 10, pp. 1131–1134, 2011.

[2] Y. Chen, W. Hong, Z. Kuai, and H. Wang, "Ku-band linearly polarized omnidirectional planar filtenna," *IEEE Antennas Wireless Propag. Lett.*, vol. 11, pp. 310–313, 2012.

[3] P. P. Shome, T. Khan, S. K. Koul, and Y. M. M. Antar, "Filtenna designs for radio-frequency front-end systems: A structural-oriented review," *IEEE Antennas Propag. Mag.*, vol. 63, no. 5, pp. 72–84, Oct. 2021.

[4] Y. C. Li, K. C. Wu, and Q. Xue, "Power amplifier integrated with bandpass filter for long term evolution application," *IEEE Microw. Wireless Compon. Lett.*, vol. 23, no. 8, pp. 424–426, Aug. 2013.

[5] X. Qi and F. Xiao, "Filtering power amplifier with up to 4th harmonic suppression," *IEEE Access*, vol. 8, pp. 29021–29026, 2020.

[6] Y. C. Li, Q.-C. Chen, Q. Xue, and J. Mou, "Filtering power amplifier with wide bandwidth using discriminating coupling," *IEEE Trans. Circuits Syst. I, Reg. Papers*, vol. 66, no. 10, pp. 3822–3830, Oct. 2019.

[7] R. Gómez-García, R. Loeches-Sánchez, D. Psychogiou, and D. Peroulis, "Single/multi-band Wilkinson-type power dividers with embedded transversal filtering sections and application to channelized filters," *IEEE Trans. Circuits Syst. I, Reg. Papers*, vol. 62, no. 6, pp. 1518–1527, Jun. 2015.

[8] Y. Deng, J. Wang, L. Zhu, and W. Wu, "Filtering power divider with good isolation performance and harmonic suppression," *IEEE Microw. Wireless Compon. Lett.*, vol. 26, no. 12, pp. 984–986, Dec. 2016.

[9] G. Zhang, X. D. Wang, J.-S. Hong, and J. Q. Yang, "A high-performance dual-mode filtering power divider with simple layout," *IEEE Microw. Wireless Compon. Lett.*, vol. 28, no. 2, pp. 120–122, Feb. 2018.

[10] S. Roshani, S. I. Yahya, B. M. Alameri, Y. S. Mezaal, L. W. Y. Liu, and S. Roshani, "Filtering power divider design using resonant LC branches for 5G low-band applications," *Sustainability*, vol. 14, no. 19, p. 12291, Sep. 2022, doi: 10.3390/su141912291.

[11] S. Roshani, S. I. Yahya, Y. S. Mezaal, M. A. Chaudhary, A. A. Al-Hilali, Y. Y. Ghadi, M. Karimi, and S. Roshani, "A compact filtering coupler with unwanted harmonic rejection using LC composite lines for communication systems applications," *Systems*, vol. 11, no. 1, p. 14, Dec. 2022, doi: 10.3390/systems11010014.

[12] J.-X. Xu and X. Y. Zhang, "Single- and dual-band LTCC filtering switch with high isolation based on coupling control," *IEEE Trans. Ind. Electron.*, vol. 64, no. 4, pp. 3137–3146, Apr. 2017.

[13] C.-L. Yang, C.-S. Lee, K.-W. Chen, and K.-Z. Chen, "Noncontact measurement of complex permittivity and thickness by using planar resonators," *IEEE Trans. Microw. Theory Techn.*, vol. 64, no. 1, pp. 247–257, Jan. 2016.

[14] L. Su, J. Munoz-Enano, P. Velez, M. Gil-Barba, P. Casacuberta, and F. Martin, "Highly sensitive reflective-mode phase-variation permittivity sensor based on a coplanar waveguide terminated with an open complementary split ring resonator (OCSRR)," *IEEE Access*, vol. 9, pp. 27928–27944, 2021.

[15] S. Kharkovsky, A. McClanahan, R. Zoughi, and D. D. Palmer, "Microwave dielectric-loaded rectangular waveguide resonator for depth evaluation of shallow flaws in metals," *IEEE Trans. Instrum. Meas.*, vol. 60, no. 12, pp. 3923–3930, Dec. 2011.

[16] A. M. Albishi, M. S. Boybay, and O. M. Ramahi, "Complementary split-ring resonator for crack detection in metallic surfaces," *IEEE Microw. Wireless Compon. Lett.*, vol. 22, no. 6, pp. 330–332, Jun. 2012.

[17] S. Deif and M. Daneshmand, "Long array of microwave sensors for real-time coating defect detection," *IEEE Trans. Microw. Theory Techn.*, vol. 68, no. 7, pp. 2856–2866, Jul. 2020.

[18] Z. Shaterian and M. Mrozowski, "Crack detection in metallic surfaces based on dumbbell-shaped defected ground structures in microstrip technology," in *Proc. 24th Int. Microw. Radar Conf. (MIKON)*, Sep. 2022, pp. 1–4, doi: 10.23919/mikon54314.2022.9924958.

[19] K. Grenier, "Recent advances in microwave-based dielectric spectroscopy at the cellular level for cancer investigations," *IEEE Trans. Microw. Theory Techn.*, vol. 61, no. 5, pp. 2023–2030, May 2013.

[20] M. H. Zarifi, H. Sadabadi, S. H. Hejazi, M. Daneshmand, and A. Sanati-Nezhad, "Noncontact and nonintrusive microwave-microfluidic flow sensor for energy and biomedical engineering," *Sci. Rep.*, vol. 8, no. 1, p. 139, Jan. 2018, doi: 10.1038/s41598-017-18621-2.

[21] K. G. Ong, C. A. Grimes, C. L. Robbins, and R. S. Singh, "Design and application of a wireless, passive, resonant-circuit environmental monitoring sensor," *Sens. Actuators A, Phys.*, vol. 93, no. 1, pp. 33–43, Aug. 2001.

[22] J. Naqui, J. Coromina, F. Martin, A. K. Horestani, and C. Fumeaux, "Comparative analysis of split ring resonators (SRR), electric-LC (ELC) resonators, and S-shaped split ring resonators (S-SRR): Potential application to rotation sensors," in *Proc. Medit. Microw. Symp. (MMS)*, Dec. 2014, pp. 1–5, doi: 10.1109/MMS.2014.7088931.

[23] A. Ebrahimi, W. Withayachumnankul, S. F. Al-Sarawi, and D. Abbott, "Metamaterial-inspired rotation sensor with wide dynamic range," *IEEE Sensors J.*, vol. 14, no. 8, pp. 2609–2614, Aug. 2014.

[24] Z. Shaterian, A. K. Horestani, and C. Fumeaux, "Rotation sensing based on the symmetry properties of an open-ended microstrip line loaded with a split ring resonator," in *Proc. German Microw. Conf.*, Mar. 2015, pp. 33–35.

[25] A. H. Karami, F. K. Horestani, M. Kolahdouz, and A. K. Horestani, "Rotation sensor based on magnetic microrods," *IEEE Sensors J.*, vol. 18, no. 1, pp. 77–82, Jan. 2018.

[26] A. H. Karami, F. K. Horestani, M. Kolahdouz, A. K. Horestani, and F. Martín, "2D rotary sensor based on magnetic composite of microrods," *J. Mater. Sci., Mater. Electron.*, vol. 31, no. 1, pp. 167–174, Jan. 2020.

[27] A. K. Horestani, Z. Shaterian, and F. Martin, "Rotation sensor based on the cross-polarized excitation of split ring resonators (SRRs)," *IEEE Sensors J.*, vol. 20, no. 17, pp. 9706–9714, Sep. 2020.

[28] A. K. Jha, A. Lamecki, M. Mrozowski, and M. Bozzi, "A microwave sensor with operating band selection to detect rotation and proximity in the rapid prototyping industry," *IEEE Trans. Ind. Electron.*, vol. 68, no. 1, pp. 683–693, Jan. 2021.

[29] J. Naqui and F. Martín, "Transmission lines loaded with bisymmetric resonators and their application to angular displacement and velocity sensors," *IEEE Trans. Microw. Theory Techn.*, vol. 61, no. 12, pp. 4700–4713, Dec. 2013.

[30] Z. Shaterian, A. K. Horestani, and C. Fumeaux, "Metamaterial-inspired displacement sensor with high dynamic range," in *Proc. 4th Int. Conf. Metamaterials, Photonic Crystals Plasmonics (META)*, Mar. 2013, pp. 274–276.

[31] A. K. Horestani, J. Naqui, D. Abbott, C. Fumeaux, and F. Martín, "Two-dimensional displacement and alignment sensor based on reflection coefficients of open microstrip lines loaded with split ring resonators," *Electron. Lett.*, vol. 50, no. 8, pp. 620–622, Apr. 2014.

[32] A. K. Horestani, Z. Shaterian, D. Abbott, and C. Fumeaux, "Application of metamaterial-inspired resonators in compact microwave displacement sensors," in *Proc. 1st Austral. Microw. Symp. (AMS)*, Jun. 2014, pp. 19–20.

[33] A. K. Horestani, J. Naqui, Z. Shaterian, D. Abbott, C. Fumeaux, and F. Martín, "Two-dimensional alignment and displacement sensor based on movable broadside-coupled split ring resonators," *Sens. Actuators A, Phys.*, vol. 210, pp. 18–24, Apr. 2014.

[34] A. K. Horestani, Z. Shaterian, and F. Martin, "Detection modalities of displacement sensors based on split ring resonators: Pros and cons," in *Proc. Int. Conf. Electromagn. Adv. Appl. (ICEAA)*, Sep. 2019, pp. 0479–0484.

[35] J. Munoz-Enano, P. Velez, L. Su, M. Gil-Barba, and F. Martin, "A reflective-mode phase-variation displacement sensor," *IEEE Access*, vol. 8, pp. 189565–189575, 2020.

[36] Z. Mehrjoo, A. Ebrahimi, and K. Ghorbani, "Microwave resonance-based reflective mode displacement sensor with wide dynamic range," *IEEE Trans. Instrum. Meas.*, vol. 71, pp. 1–9, 2022, doi: 10.1109/TIM.2021.3130669.

[37] A. K. Horestani, Z. Shaterian, and M. Mrozowski, "High dynamic range microwave displacement and rotation sensors based on the phase of transmission in groove gap waveguide technology," *IEEE Sensors J.*, vol. 22, no. 1, pp. 182–189, Jan. 2022.

[38] Z. Shaterian and M. Mrozowski, "Displacement sensors based on the phase of the reflection coefficient of a split ring resonator-loaded transmission line," *IEEE Sensors J.*, vol. 22, no. 21, pp. 20321–20327, Nov. 2022.

[39] A. K. Horestani, Z. Shaterian, and M. Mrozowski, "Microwave alignment and displacement sensors in groove gap waveguide technology," in *Proc. 52nd Eur. Microw. Conf. (EuMC)*, Sep. 2022, pp. 828–831.

[40] C.-H. Chio, K.-W. Tam, and R. Gomez-Garcia, "Filtering angular displacement sensor based on transversal section with parallel-coupled-line path and U-shaped coupled slotline," *IEEE Sensors J.*, vol. 22, no. 2, pp. 1218–1226, Jan. 2022.

[41] Z. Shaterian and M. Mrozowski, "A multifunctional microwave filter/sensor component using a split ring resonator loaded transmission line," *IEEE Microw. Wireless Technol. Lett.*, vol. 33, no. 2, pp. 220–223, Feb. 2023.

[42] D. M. Pozar, *Microwave Engineering*. Hoboken, NJ, USA: Wiley, 2011.

[43] J.-S. G. Hong and M. J. Lancaster, *Microstrip Filters for RF/Microwave Applications*. Hoboken, NJ, USA: Wiley, 2004.

ZAHRA SHATERIAN (Member, IEEE) received the B.Eng. degree from the Amirkabir University of Technology, Iran, in 2004, the M.Eng. degree from the K. N. Toosi University of Technology, Iran, in 2007, and the Ph.D. degree (Hons.) with a minor in computational electromagnetics from The University of Adelaide, Adelaide, SA, Australia, in 2015, all in electrical and electronics engineering.

She was a recipient of the Dr. Chamran Prize from the Iran National Elites Foundation, under which she served as a Postdoctoral Researcher at the University of Tehran, from 2016 to 2018. Since 2018, she has been with the Faculty of Shariaty, Technical and Vocational University (TVU), where she is currently an Assistant Professor. She is also a Postdoctoral Researcher with the Gdańsk University of Technology, Poland. Her research interests include computational electromagnetics, time-domain meshless methods, metamaterials and their applications, microwave sensors, and gap waveguide technology.

Dr. Shaterian received the Best Paper Award from the International Symposium on Electromagnetic Compatibility, in 2014; and the two Best Student Paper Awards from the International Workshop on Antenna Technology, in 2014, and the Australian Microwave Symposium, in 2014. She was the winner of the 2015 Gertrude Rohan Memorial Prize and the Medal for the Best Ph.D. Thesis in the areas of information and communication technology and also received the 2014 Simon Rockliff Award for outstanding postgraduate mentorship.

MICHAL MROZOWSKI (Fellow, IEEE) received the M.Sc. degree (Hons.) in telecommunication engineering and the Ph.D. degree (Hons.) in electronic engineering from the Gdańsk University of Technology, in 1983 and 1990, respectively.

In 1986, he joined the Department of Electronics, Gdańsk University of Technology, where he is currently a Full Professor, the Head of the Department of Microwave and Antenna Engineering, and the Director of the Doctoral School. He has published one book and over 100 peer-reviewed articles in IEEE journals. He has developed several software modules that have been then integrated into commercial microwave EDA software used all over the world. His research interests include computational electromagnetics, photonics, and microwave engineering. His current work is focused on the development of new fast numerical techniques for solving 2-D and 3-D boundary value problems in the time and frequency domains, automated microwave filter design, microwave filter synthesis, microwave sensor design, microwave EDA, reduced-order models for grid-based numerical techniques (e.g., FDTD and FEM), and surrogate model construction.

Prof. Mrozowski was a member of Editorial Board of the PROCEEDINGS OF THE IEEE. He currently serves as a member of Editorial Board for IEEE ACCESS. He is a member of the MTT-1 and MTT-2 Technical Committees, a fellow of the Electromagnetics Academy, and a member of the Polish Academy of Sciences. He was a past Vice-Dean for research of the ETI Faculty and the past Chairperson of the Polish AES/AP/MTT Chapter. He served as an Associate Editor for IEEE MICROWAVE AND WIRELESS COMPONENTS LETTERS.